14th International Symposium on Turbulence and Shear Flow Phenomena (TSFP14)
Heidelberg, Germany, July 28–31, 2026

LES OF SUPERSONIC AIR INLET BUZZ PHENOMENON WITH A LAMINAR VS TURBULENT BOUNDARY LAYER ON THE EXTERNAL COMPRESSION RAMP

Stéphane Jamme*, **Samuel Deleu, Marc Montagnac, Romain Gojon and Jérémie Gressier**
ISAE-SUPAERO, University of Toulouse, France
*email: stephane.jamme@isae-supaero.fr

ABSTRACT

This paper investigates the flow in a supersonic mixed-compression air intake using Large Eddy Simulation. We study an off-design regime where strong flow instabilities (big buzz phenomenon) develop due to the throttling of the air inlet at the end of the diffuser. In a first step, we investigate the sensitivity of the big buzz to the laminar vs turbulent nature of the boundary layer on the external ramp. Then, we analyze the physical mechanisms responsible for the observed behaviour of the flow.

INTRODUCTION

Aerobic propulsion systems require sufficient airflow through the engine to operate nominally. The design of the air inlet then plays a key role in the performance of the propulsion system. This is particularly true in the supersonic flight regime where the incoming flow must be decelerated before entering the core of the engine. Supersonic flight implies the presence of compressible phenomena such as shock waves and expansions from the ramp compression devices or from the inlet cowl lip. The latter can impact the boundary layers developing on the opposite walls. These shock wave/boundary layer interactions (SBLI), which vary according to flight conditions, have direct repercussions on the performance and operation of the supersonic air inlet (Chen *et al.* (2018)). They introduce strong adverse pressure gradients that may cause separation of the boundary layers. The air flow rate is then reduced, which is detrimental to the propulsion system.

One major well-known problem of these configurations is the supersonic inlet buzz (Oswatitsch (1947)) which can be a great threat to air-breathing supersonic vehicles. Usually, it is triggered by an accidental downstream pressure- or thermal-driven flow blockage, which can cause the inlet to enter the undesirable subcritical mode featuring the expected terminal shock standing upstream of the inlet entrance. Once buzz occurs, self-excited streamwise normal-shock oscillations are generated along with periodic duct pressure fluctuations, provoking a sharp drop in captured air flow and the consequent engine thrust penalty. Inlet buzz with intense fluid unsteadiness should thus be avoided as much as possible.

The efficient design of supersonic air inlets is still a challenge today, and performing numerical simulation of such flow configurations is a difficult task due to the unsteady turbulent nature of the problem and the presence of turbulence, shocks and acoustic waves that interact with each other. One possible approach is to perform Large Eddy Simulations (LES) of this complex flow. However, given the sensitivity of SBLI to the laminar vs turbulent nature of the boundary layer, it is expected that the buzz phenomenon also depends on this feature of the flow. The objective of the present work is to investigate this point in the context of big buzz producing large oscillations of the shock system. We compare two LES of the same big buzz configuration which differ only in the turbulent or non-turbulent nature of the boundary layer on the external compression ramp. In a second step, we also analyze the physical mechanisms responsible for the observed behaviour of the flow.

NUMERICAL SETUP

Configuration and numerical method

The present wall-resolved compressible LES were performed using our in-house IC3 solver, which solves the spatially filtered compressible Navier-Stokes equations for conserved quantities using a finite volume formulation on unstructured meshes. An explicit third-order Runge-Kutta scheme is used for time advancement. The solver relies on Vreman (2004) subgrid-scale model to represent the influence of unresolved small-scale fluid motions. It also features a solution-adaptive methodology which combines a low-dissipative centered numerical scheme and a first-order upwind scheme in regions of the flow where discontinuities are present. For this purpose, a DVPG shock sensor based on the values of dilatation β, vorticity ω and pressure gradient ΔP, is used to identify the presence of discontinuities in the flow: in the cells where the ratio $\mathrm{DVPG} = \frac{\beta}{\omega}\frac{\Delta P}{P}$ exceeds a threshold value to be tuned, the first order scheme is applied while in the other cells, the low-dissipative scheme is kept.

The geometry of the air inlet selected in the present work can be seen in Figure 1. It has been used in Chen *et al.* (2018) experiments. The upstream flow is characterized by a Mach number of $M = 2.41$, a total pressure of 100.9 kPa, a total temperature of 294.1 K, and a Reynolds number, based on the upstream quantities and the height $h = 47.5$ mm of the final straight portion of the air inlet duct, equal to 247320. The spanwise extent of the computational domain has been set to $L_z = \delta_0$, where $\delta_0 = 2.4$ mm is the size of a turbulent boundary layer (estimated using the 1/7$^{\text{th}}$ power law) developing with no pressure gradient on the bottom ramp of the inlet, up to the point where the bow shock generated by the cowl lip impacts the bottom wall. This results in a ratio of $\delta_0/h = 0.05$ for the thickness of the ramp boundary layer at the first interaction with the cowl-induced shock wave.

The back-pressure imposed at the exit can be increased in order to mimic a blockage due to the presence of a downstream

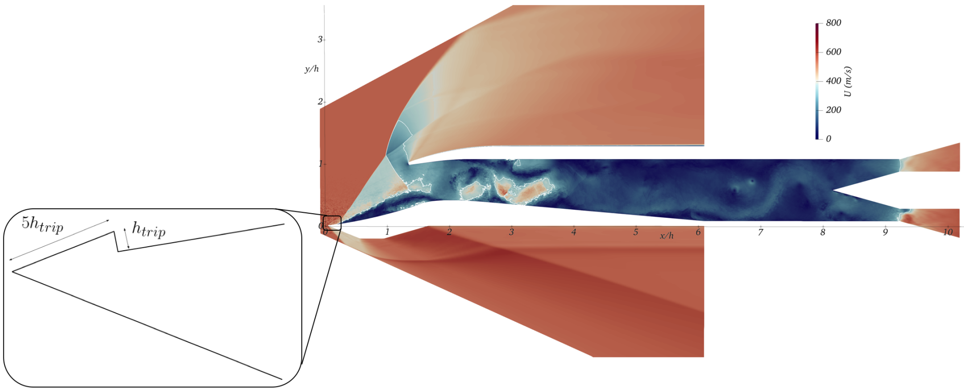

Figure 1: 2D Snapshot of velocity magnitude for the *TR*=0.6 tripped case (sonic lines are depicted in white) with detail of the geometrical modification introduced at the ramp tip. Note that the upper and lower parts of the numerical domain are cropped in the figure.

engine. This is achieved by placing a plug at the exit of the air inlet duct (see Figure 1). The plug reduces the massflow and leads to an increase of the back-pressure which modifies the operating point of the air inlet. This procedure allows investigating different flow regimes of the air inlet, ranging from steady configurations for the mean flow to fully unsteady behaviors featuring the buzz phenomenon. In order to quantify the downstream blockage, a throttling ratio (*TR*) is defined as $TR = 1 - A_{th,plug}/A_{exit}$, where $A_{th,plug}$ is the throat area near the plug and A_{exit} is the cross-sectional area of the duct exit. In this work, we concentrate on a “big buzz” configuration corresponding to *TR*=0.6 (no blockage corresponds to *TR*=0).

The computational grid is refined close to the ramp and cowl walls, as well as in the core region in the vicinity of the entrance of the air intake. The size of the cells has been chosen such as $4 < \Delta x^+ < 84$, $\Delta y^+ = 1$ and $\Delta z^+ = 15$, enabling wall-resolved LES. All variables of the supersonic flow are specified at the inlet boundary of the domain (vertical left and top/bottom oblique boundaries), while a relaxed pressure outlet boundary condition is used for outlets (vertical right boundaries). The ramp and cowl walls of the air inlet are set as adiabatic no-slip walls, while the plug walls are set to adiabatic slip walls when present ($TR \neq 0$), to reduce the numerical cost of the simulations. Periodic boundary conditions are used in the spanwise direction.

Cases considered

Four cases are considered in our study. Two unthrottled configurations (*TR*=0) permitting to validate the numerical setup, and two simulations with the plug (*TR*=0.6). For each of these two *TR* values, a simulation without specific treatment to trigger the transition of the boundary layer on the external ramp of the air intake is first performed. This results in a fully laminar boundary layer as illustrated in Figure 2 (top) for a case without plug ($TR = 0$). Then, an additional simulation is conducted where the ramp boundary layer is forced to a turbulent state, see Figure 2 (bottom), by the combination of two ingredients: the introduction of a geometrical trip at the tip of the ramp and the injection of freestream homogeneous isotropic turbulence (HIT) at the inlet of the domain in front of the ramp. This allows to also take advantage of the by-pass transition mechanism. The combination of these two approaches has been found to be the optimal way to trip the ramp boundary layer (Deleu *et al.* (2023)).

The geometrical trips were designed based on the work of De Tullio *et al.* (2013). The flow conditions observed in this study are indeed the closest to those studied here, as they investigate the influence of roughness elements over a compressible boundary layer at Mach number $M = 2.5$. A rectangular geometry for these appendices was initially tested, but was abandoned because it accentuates the oblique shock wave associated with the deflection imposed by the ramp, which has a significant impact on the downstream flow and is thus undesirable. It was therefore decided to replace the rectangular trip with a triangular one ending in a sharp edge (see insert in Figure 1). It indeed appears that the separation imposed by the downward step on the downstream part of the trip is the main cause of the boundary layer transition.

In order to take advantage of the bypass transition, turbulent fluctuations were superimposed on the mean flow in the inlet plane to target a specific turbulence intensity Tu. The integral length scale of the turbulence l_t was set to $l_t = 0.5$ mm,

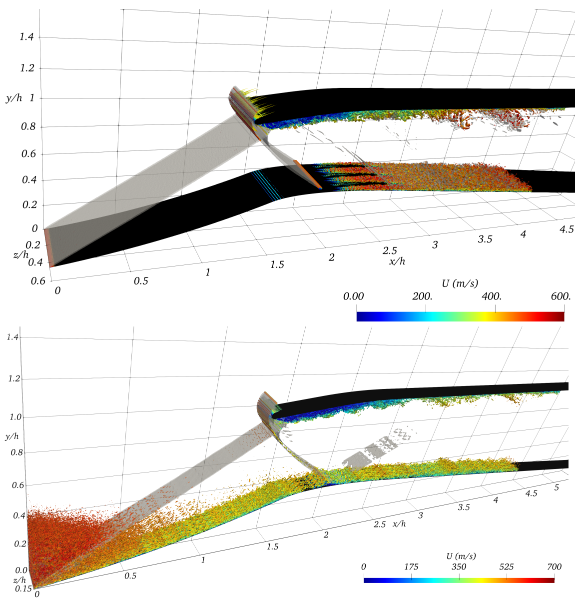

Figure 2: 3D Iso Q-criterion colored by the longitudinal velocity and contours of M = 1 characterizing the shock structures (the simulation domain has been replicated three times in the spanwise direction). Top: *TR*=0 case without tripping; Bottom: *TR*=0 case with tripping.

which is approximately three times the height of the trip considered.

Several trip heights and several Tu values for the HIT input were tested in order to find the optimal configuration and achieve the most efficient transition of the boundary layer ramp, see Deleu *et al.* (2023). Overall, the combination of a triangular-shaped trip with a height of $h_t = 0.22 \cdot \delta_{99} = 0.175$mm (where δ_{99} corresponds to the thickness of a laminar boundary layer at the end of the ramp) and an inlet HIT corresponding to $Tu = 8\%$, was chosen as the most favorable configuration to trigger the boundary layer towards a realistic turbulent state.

The computational meshes used in this work involve $53 \cdot 10^6$ cells for the *TR*=0.6 case without trip and $76 \cdot 10^6$ cells for the tripped *TR*=0.6 case.

RESULTS

Comparison between the tripped and untripped cases

When comparing the behaviour of the flow between the *TR*=0 case and the *TR*=0.6 cases (tripped or not), the inception of a strong unsteadiness on the external ramp in the throttled cases is striking. This is clearly illustrated in Figure 1 where a massive separation can be observed on the ramp for *TR*=0.6, while an attached development of the ramp boundary layer occurs in the *TR*=0 case with steady shock waves, see Figure 2.

The strong unsteady nature of the shocks in the throttled cases is characterized by an oscillating behavior of the flow operating in the undesirable subcritical regime of the intake and corresponding to the so-called big buzz phenomenon. Figure 3 displays space-time maps of instantaneous pressure along a line of probes positioned at $y/h = 0.5$ and covering almost the entire length of the diffuser in the longitudinal direction (*i.e.* $0 < x/h < 7.4$ - note that the plug throat section at the end of the diffuser is located at $x/h = 9.3$).

On the left of Figure 3 (top), for the *TR*=0.6 untripped case, regular back-and-forth oscillations of the separation shock wave are observed and correspond to the wavy trajectory displayed on the left side of the map. This is accompanied by strong oscillations of the massflow entering the inlet diffuser, here calculated in a section of the duct taken at $x/h = 1.91$. A regular cyclic behaviour takes place in this case. Due to the strong adverse back-pressure introduced by the presence of the plug, the angle of the ramp tip shock gradually straightens out and the separation on the ramp increases in size up to the point where a large-scale vortical structure detaches, leading to a serious blockage of the air inlet duct (see red inserts in Figure 3, top) and a drop of the ingested massflow. This vortical structure is subsequently advected into the diffuser and the shrunk separation region on the ramp starts to increase again.

In the tripped *TR*=0.6 case (Figure 3, bottom), the same kind of oscillatory behavior is observed, but the oscillations appear in a first step less regular than in the previous case. In particular, the intensity of the vortex structures emissions varies so that these vortices do not always impinge on the upper cowl lip (see green inserts). These moderate events seem to alternate with stronger ones (see red inserts) similar to those reported in the untripped *TR*=0.6 case, thus disrupting their regular frequency of occurrence. However, after this transient period, the oscillatory behaviour of the flow becomes more regular, with only strong emissions impinging on the cowl lip for $\frac{tu_0}{h} > 200$, where $u_0 = 564$ m/s corresponds to the freestream upstream velocity. From that moment on, both the untripped and tripped *TR*=0.6 simulations follow the same trend in terms of flow organization and characteristic frequencies of the big buzz phenomenon. The laminar/turbulent state of the boundary layer on the external ramp thus makes no clear difference for this strongly throttled configuration. However, it can be noted that the ingested massflow is less sinusoidal in the tripped case, as compared with the untripped one. Moreover, at each cycle, an almost null massflow is reached for a short duration.

Physical mechanism of the big buzz

When looking at Figure 3, one can observe multiple travelling waves whose footprint corresponds to the oblique lines that emerge from the background activity. Since in compressible fluid flow, the information generally propagates at the

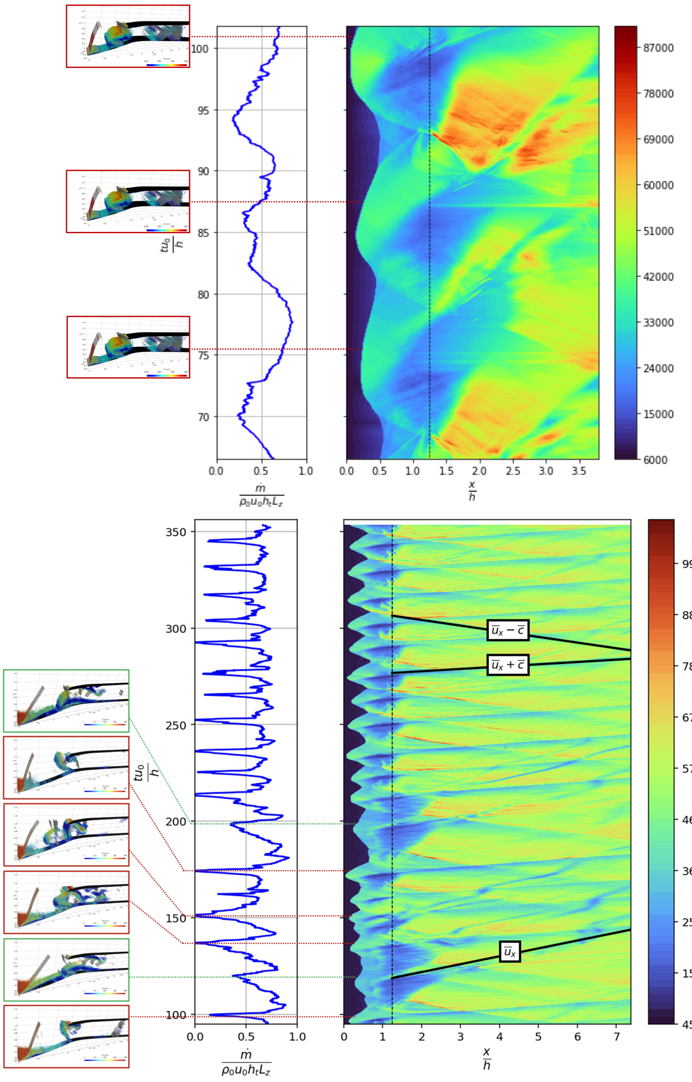

Figure 3: Axial position vs time diagram of pressure signal [Pa] on a line probe located at $y/h = 0.5$, *TR*=0.6 case. Top: case without tripping ; Bottom: case with tripping. The vertical dashed line indicates the position of the upper cowl lip. The evolution of the massflow entering the diffuser of the inlet is also reported aside the (x-t) map. Inserts show events of vortical structures emissions emanating from the massive separation on the ramp: strong events in red boxes, moderate events in green boxes (Q-criterion is used).

one-dimensional characteristic velocities u_x, $u_x - c$ and $u_x + c$, with u_x the longitudinal convection velocity and c the speed of sound, we plot the mean values of these velocities in Figure 4 along the investigated line of probes. An average is then performed along the internal duct and the result is taken as an approximation of the one-dimensional value of the characteristic velocities that are reported in Figure 3 (bottom) and Figure 5. It is clear that the slopes of the main travelling waves closely match the calculated characteristic velocities.

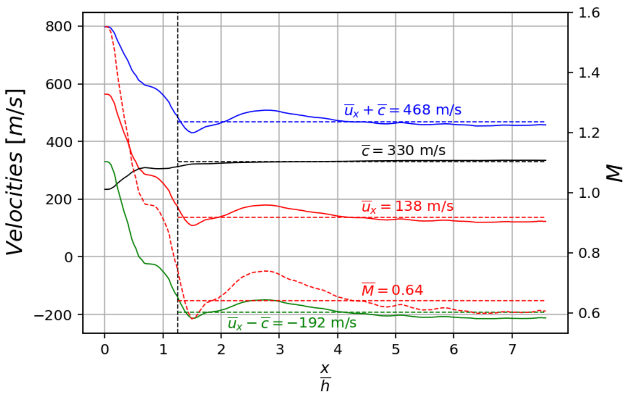

Figure 4: Mean propagation velocities and Mach number along the duct of the air inlet (same probing line as in the pressure maps). The vertical dashed line indicates the position of the upper cowl lip.

In order to investigate more precisely the flow mechanisms underlying the observed big buzz phenomenon, we concentrate on a shorter time interval taken from the range corresponding to the regular behaviour observed in the *TR*=0.6 tripped case. This time interval corresponds to the range $270 < \frac{tu_0}{h} < 320$, and the corresponding close-ups on the time maps of the instantaneous and fluctuating pressures are displayed in Figure 5. We report on this figure six specific instants taken inside one period of the massflow oscillations, labelled with letters (a), (b), (c), (d), (e) and (f). Instantaneous 2D snapshots (taken in the transverse mid-plane of the domain) of the actual flow field corresponding to these six instants are presented in Figure 7.

The big buzz cycle presented in these figures starts at an instant (a) when the ramp-side flow is massively separated due to the strong adverse back-pressure introduced by the presence of the plug, with the corresponding separation shock located at its most upstream position on the wavy trajectory of the ramp shock displayed in Figure 5. At this instant, the separation bubble breaks down into a large-scale clockwise-rotating structure that causes the maximum obstruction to air intake diffuser at instant (b) when the minimum massflow is observed. The backward advection of this vortex is accompanied by the inception of a compression wave that propagates downstream inside the duct at a velocity of $\bar{u}_x + \bar{c}$ and by the retractation of the separation shock on the ramp towards the air inlet duct section. The large-scale separated vortical structure subsequently impinges on the cowl lip before being partly ingested into the diffuser and partly spilled over the cowl (c). This leads to an increase of the massflow entering the air inlet and a strengthening of the compression wave propagating downstream. The reflected compression wave on the cowl lip then bounces back upstream and also reflects on the ramp wall generating an additional forward-propagating compression wave (c). These two waves interact with the retracting separation shock and cause the shock wave to stop its downstream motion. An additional compression wave coming from the end of the inlet duct then hits the shock immediately afterwards, sending it back towards the front $(d-e)$. Between instants (c) and (d), during the retractation phase of the shock, the separated region on the ramp has a moderate size and the ingested massflow increases and reaches its maximum value close to instant (e), immediately after the shock rebounds forwards. Afterwards, the shrunk separation region on the ramp starts to increase again $(d-e)$. This process keeps on going and the progressive increase of the extent of the separation region gradually induces a steepening of the separation shock wave and a return to the beginning of the cycle (f).

The frequency associated to the massflow oscillations, also corresponding to the frequency of the back-and-forth motion of the separation shock on the external ramp, has been estimated to be close to 900 Hz ($St = fh/u_0 = 0.076$). Furthermore, the propagation time of the compression wave travelling to and from the x-coordinate corresponding to the point furthest upstream of the separation shock has been estimated to $3.3 \cdot 10^{-3}$ s, which corresponds to a frequency close to 300 Hz ($St = fh/u_0 = 0.0252$). We can therefore observe three cycles of buzz during one travel period of this compression wave, as illustrated in Figure 5.

The characteristic frequencies of the flow are displayed in Figure 6 that corresponds to the FFT map of pressure along the investigated line of probes. The frequency associated to the motion of the shock wave on the ramp ($St = fh/u_0 = 0.076$) is clearly visible in the range $0 < x/h < 0.5$. It can also be found near the entrance of the diffuser where the large-scale emitted structures are periodically ingested inside the duct, as well as within the latter, but with a weaker imprint. The lowest peak at $St = 0.0042$ corresponds to the FFT resolution limit and has no physical significance. A smeared spot around 150 Hz ($St = 0.0126$) can also be observed just after the duct entrance ($x/h \approx 1.5$) and seems to correspond to the frequency of the moderate structures emissions highlighted in Figure 3 (bottom) for $\frac{tu_0}{h} < 200$, before the establishment of the more regular oscillatory behaviour of the flow.

In the literature, we generally find scenarios based on acoustic loop models (Newsome, 1984; Trapier *et al.*, 2006) relying on the acoustic modes ($n = 1, 2, 3...$) of an open-closed duct whose frequency is given by the following formula:

$$f_n = (2n-1)\frac{c}{4L}(1-M^2) \tag{1}$$

where M is the mean Mach number and c the mean speed of sound inside the diffuser. The throat at the plug side is generally considered as acoustically closed since it is choked, while the aperture of the air inlet is considered open despite the presence of the oblique shock. Equation (1) assumes a uniform distribution of both M and c in the duct, which is not the case in the present configuration. However, if we consider from the LES fields that a mean Mach number of $\overline{M} = 0.64$ and a mean speed of sound of $\bar{c} = 330$ m/s are representative of the flow inside the air inlet (see Figure 4), and taking a duct length of $L = 8h$ (distance between the inlet section of the diffuser and the throat of the plug), we obtain from equation (1) a fundamental frequency of the open-closed duct equal to $f_{n=1} = 128$ Hz ($St_{n=1} = 0.0107$). This fundamental frequency is slightly visible in the FFT map presented in Figure 6. How-

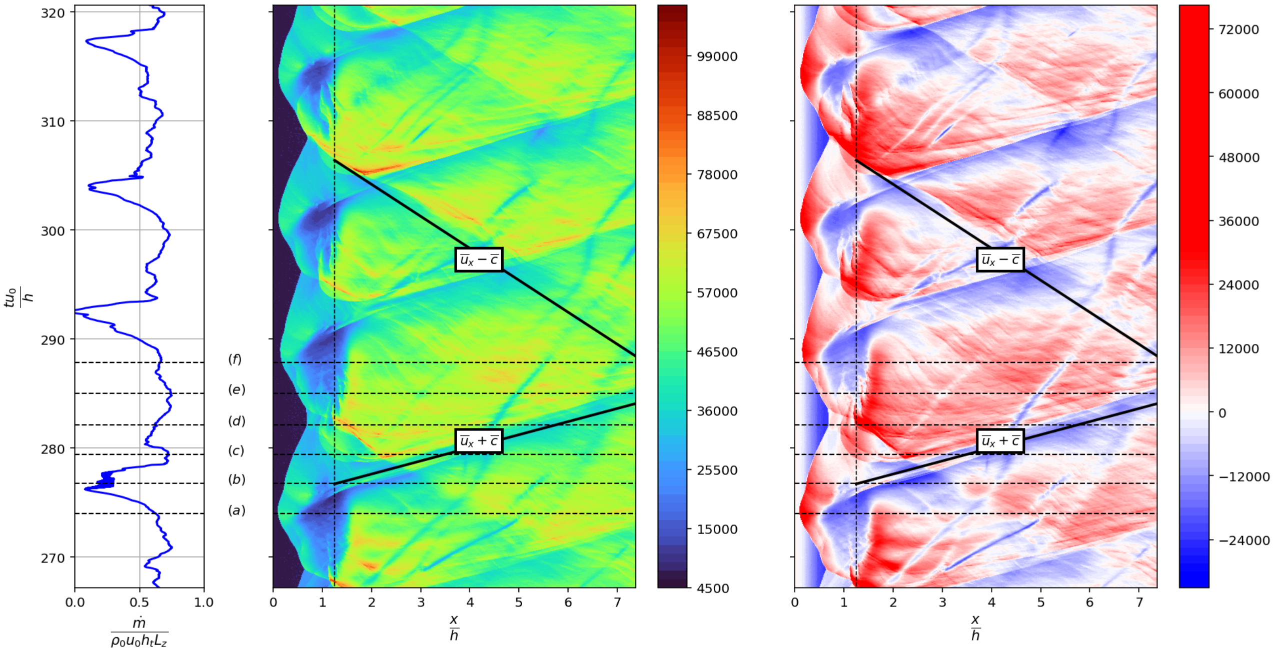

Figure 5: Axial position vs time diagram of pressure signals [Pa] on a line probe located at $y/h = 0.5$, tripped *TR*=0.6 case, zoom inside the "established" buzz regime. Left: instantaneous pressure ; Right: fluctuating pressure. The vertical dashed line indicates the position of the upper cowl lip. The evolution of the massflow entering the diffuser of the inlet is also reported aside the (x-t) map.

ever the third and fourth harmonics corresponding respectively to 384 Hz ($St_{n=3} = 0.054$) and 896 Hz ($St_{n=4} = 0.075$) are much clearer both on the external ramp and inside the air inlet diffuser. This means that the acoustic feedback loop scenario is indeed present in the big buzz configuration under investigation.

The intense buzz phenomenon appears to be triggered by the large separated flow region on the external compression ramp, which obstructs the inlet entrance. All subsequent shock movements and pressure fluctuations are then driven by acoustic pressure waves traveling back and forth within the diffuser, synchronizing the buzz to a regular frequency that matches the acoustic resonance modes of the diffuser. However, the measured buzz oscillation frequency does not align with the fundamental mode but instead corresponds to higher harmonics. As suggested by Dailey (Dailey, 1954), this behavior may be linked to vortex shedding from the cowl lip, which can be observed in Figure 7 on the upper section of the diffuser. These vortices originate from the recurrent impact of large separated flow structures, formed on the ramp, against the cowl lip, and travel inside the diffuser. This flow perturbation preferentially excites modes 3 and 4 of the diffuser, forcing the system to oscillate at higher harmonic frequencies rather than the fundamental tone. This indicates that the intense buzz phenomenon investigated in this study is a coupled interaction between hydrodynamics and acoustics waves, with two different synchronized feedback loops.

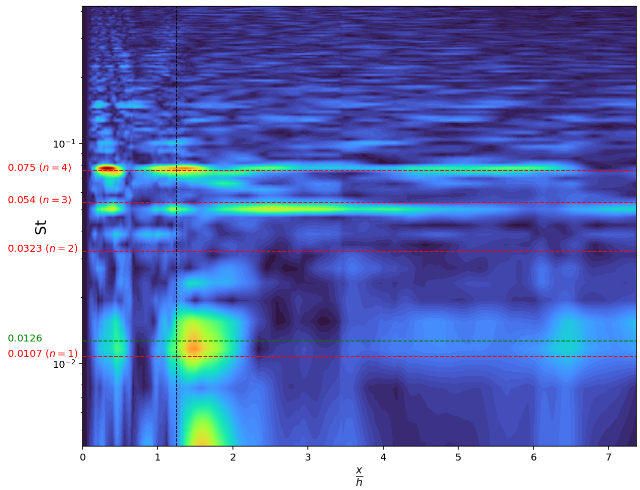

Figure 6: Axial position vs frequency diagram of the norm of the FFT coefficient of the pressure signal on the investigated line probe, tripped TR60 case. Colormap: arbitrary scale. Horizontal dotted lines display characteristic frequencies of the configuration.

ACKNOWLEDGMENTS

This work was granted access to computing and storage resources by GENCI at TGCC thanks to the grant 2026-A0182A07178 on the supercomputer Joliot Curie's ROME partition. We acknowledge EuroHPC JU for awarding the project ID EHPC-REG-2023R03-113 access to MeluXina at LuxProvide, Luxembourg.

REFERENCES

Chen, Hao, Tan, Hui-Jun, Zhang, Qi-Fan & Zhang, Yue 2018 Throttling process and buzz mechanism of a supersonic inlet at overspeed mode. *AIAA Journal* **56** (5), 1953–1964.

Dailey, C. L. 1954 Supersonic diffuser instability. Phd thesis, California Institute of Technology, Pasadena, CA (USA).

De Tullio, N., Paredes, P., Sandham, N. D. & Theofilis, V. 2013 Laminar-turbulent transition induced by a discrete roughness element in a supersonic boundary layer. *Journal of Fluid Mechanics* **735**, 613–646.

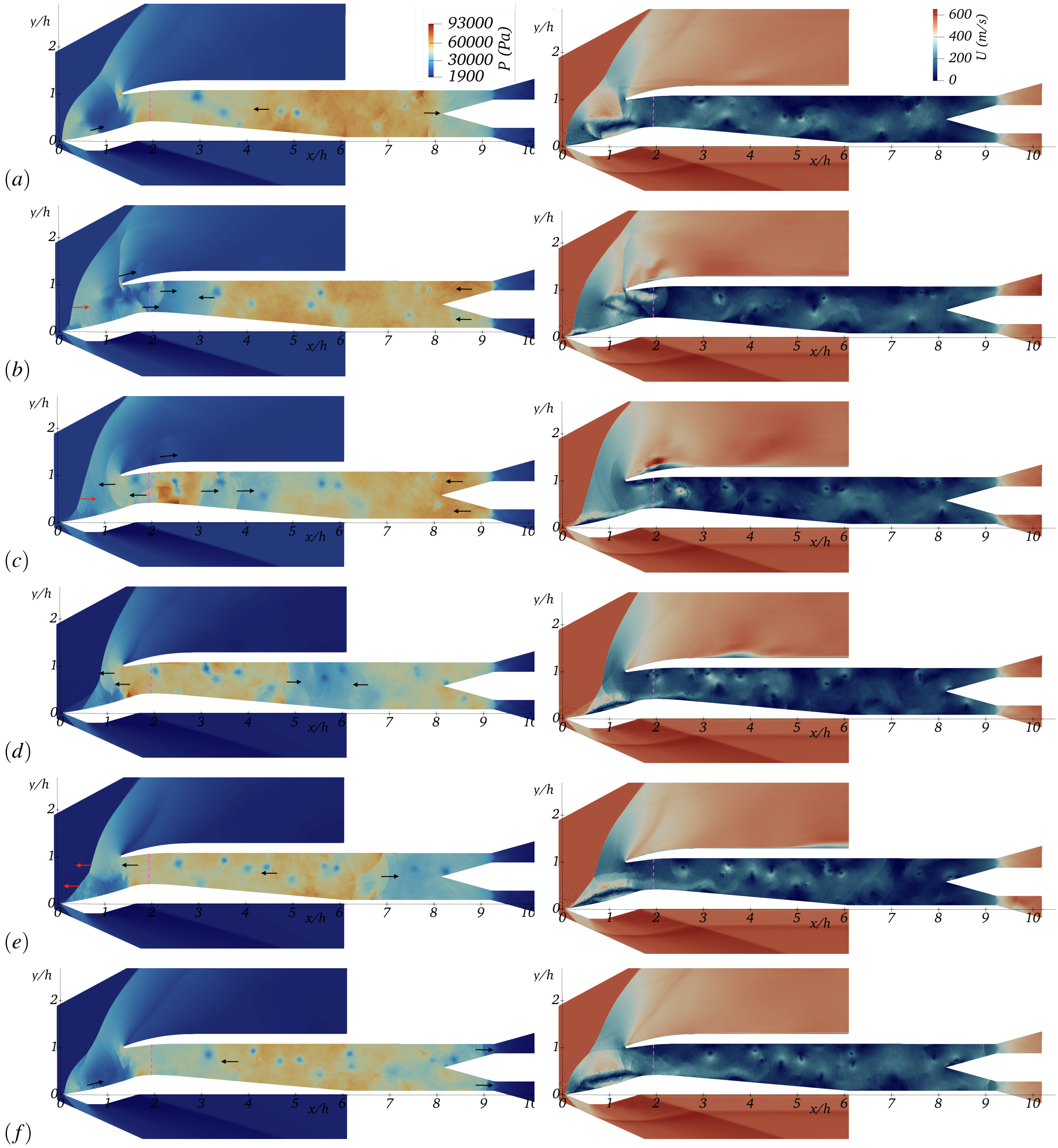

Figure 7: Instantaneous 2D snapshots of pressure (left column) and velocity magnitude (right column) for the different characteristic instants of one big buzz cycle (see Figure 5). Red and black arrows indicate, respectively, the direction of propagation of the separation shock wave on the ramp and that of the main pressure waves inside the diffuser of the air inlet. The vertical purple dashed line corresponds to section $x/h = 1.91$ where the massflow is calculated.

Deleu, Samuel, Sanchez-del Rio, Alvaro, Gojon, Romain, Gressier, Jérémie & Jamme, Stéphane 2023 Boundary layer tripping effects on supersonic air inlet buzz phenomenon. In *13rd Int. Symp. on Turbulence and Shear Flow Phenomena*.

Newsome, R.W. 1984 Numerical simulation of near-critical and unsteady, subcritical inlet flow. *AIAA Journal* **22** (10), 1375–1379.

Oswatitsch, K. 1947 Pressure recovery for missiles with reaction propulsion at high supersonic speeds. *NACA 1140* .

Trapier, S., Duveau, P. & Deck, S 2006 Experimental Study of Supersonic Inlet Buzz. *AIAA Journal* **10** (10), 2354–2365.

Vreman, A.W. 2004 An eddy-viscosity subgrid-scale model for turbulent shear flow: Algebraic theory and applications. *Physics of fluids* **16** (10), 3670–3681.